Rapid Communications

Twinning path determined by broken symmetry: A revisit to deformation twinning in hexagonal close-packed titanium and zirconium

Yipeng Gao [1,*] Jia-Hong Ke [1] Bo Mao [2] Yiliang Liao [2] Yufeng Zheng [3] and Larry K. Aagesen [1]

[1] *Department of Computational Mechanics and Materials, Idaho National Laboratory, 955 MK Simpson Boulevard, Idaho Falls, Idaho 83415, USA*

[2] *Department of Mechanical Engineering, University of Nevada Reno, 1664 North Virginia Street, Reno, Nevada 89557, USA*

[3] *Department of Chemical & Materials Engineering, University of Nevada Reno, 1664 North Virginia Street, Reno, Nevada 89557, USA*

(Received 31 March 2020; revised 27 May 2020; accepted 19 June 2020; published 6 July 2020)

Deformation twinning is one of the major deformation mechanisms in crystals, which plays an important role in determining the mechanical properties of metals and alloys. One of the important issues to understand twinning mechanisms is the determination of the deformation path. However, due to a lack of theoretical tools, a fundamental relationship between symmetry breaking and the deformation path has not been established in materials science, which conceals the physical origin of deformation twinning. Utilizing a graph approach for deformation pathways, we show that twinning modes in hexagonal close-packed (hcp) titanium and zirconium are dictated by both the symmetry of hcp and the symmetry breaking associated with the bcc to hcp transformation. Our work not only opens another avenue to investigate the symmetry and symmetry breaking in hcp crystals, but also provides insight into the physical origin of crystalline defects.

DOI: 10.1103/PhysRevMaterials.4.070601

I. INTRODUCTION

Deformation twinning is one of the most important deformation mechanisms in crystals, which has been widely identified in a variety of crystals, including typical face-centered-cubic (fcc), body-centered-cubic (bcc), and hexagonal close-packed (hcp) metals/alloys as well as ordered intermetallic compounds [1–4]. Deformation twinning is especially important in crystals of lower symmetry (e.g., hcp, orthorhombic) where the five independent slip systems required for a general deformation are unavailable [5,6], and becomes the dominant deformation mode as temperature is lowered or strain rate is increased [1,4]. From both scientific and engineering points of view, the determination of the twinning mode is the foundation for the calculations of twinning strain and critical shear stress, which are critical material parameters for the prediction of the mechanical behavior of metals and alloys [1].

In the literature, a number of mathematical parameters have been introduced to unambiguously describe a twinning mode [1,7], including (i) twin plane, (ii) twinning shear vector, and (iii) misorientation between two twin-related domains. Note the relation among the three parameters. From a theoretical point of view, parameters (i) and (ii) are sufficient to define a twinning mode unambiguously, while parameters (iii) can be determined by the given (i) and (ii). From an experimental point of view, (i) and (iii) can be directly measured through transmission electron microscopy and electron backscatter diffraction techniques, while parameter (ii) is difficult to directly identify unless an *in situ* atomic resolution observation is available. However, a twinning mode cannot be uniquely determined through (i) and (iii). As a typical example, we consider a $\Sigma 3$ twin on a $\{112\}$ plane in bcc. Note that $\{112\}$ is the twin plane (i), while $\Sigma 3$ is the misorientation (iii), i.e., a 60° rotation about $\langle 111\rangle$ (or a 70.5° rotation about $\langle 110\rangle$). In the literature, two different twinning paths have been proposed, both of which lead to $\Sigma 3$ twin boundaries on $\{112\}$ [1]. In Fig. 1, the paper plane is $(01\bar{1})$ in the bcc index. Blue and orange atoms are on different $(01\bar{1})$ planes, which indicates an ABABAB … stacking sequence along the $[01\bar{1}]$ direction. An initial undeformed rectangular domain is colored red. After the twinning, one half of the domain (lower right triangle) transforms to twin (colored green), with a (211) twin plane. As reported in the literature [1], there are two twinning mechanisms providing exactly the same twin plane and misorientation (shown in Fig. 1). The two mechanisms have opposite shear vectors, with their conjugate twin planes being $\{112\}$ and $\{332\}$, respectively [1]. In principle, both twinning modes could exist in reality, i.e., it is possible that they exist in different bcc metals such as Mo and Ti. However, they cannot be distinguished based on the experimental results of (i) and (iii) alone.

It is a general crystallographic phenomenon that different twinning paths can lead to identical twin boundaries and misorientation, which also exists in hcp crystals. For example, at least two different twinning paths have proposed in the literature for the $\{11\bar{2}2\}$ twin, with different shear vectors and different conjugate twin planes [1,8–10], and it is still a controversial issue to determine the twinning mechanism for the $\{11\bar{2}2\}$ twin. Because of a large number of possible twinning modes through different combinations of atomic shears and shuffles [1,8–14], such an ambiguity exists for most of the typical twin modes in hcp. As will be shown in

*Corresponding author: yipeng.gao@inl.gov

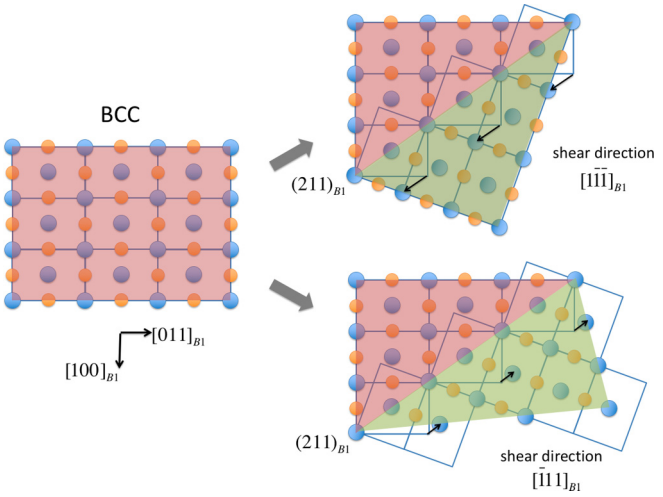

FIG. 1. The change in atomic structure for two different deformation twinning mechanisms that leads to the same twin plane and misorientation in bcc. The shear vectors (indicated by black arrows) are opposite for the two twinning modes. (Viewing direction: $[01\bar{1}]$ in bcc.)

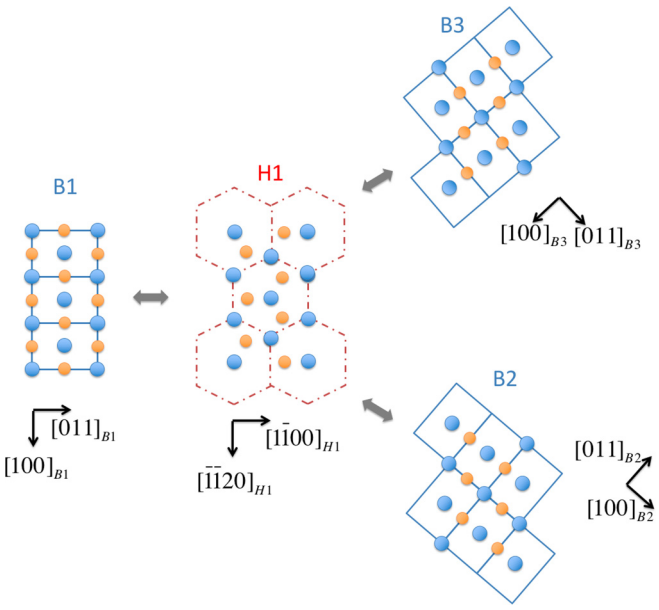

FIG. 2. The change in crystal structure during the hcp → bcc transformation. From a single hcp state (H1), three equivalent bcc states (B1, B2, and B3) can be generated by the transformation through Burgers correspondence. (Viewing direction: $[01\bar{1}]$ in bcc and [0001] in hcp.)

our results, the deformation paths for $\{10\bar{1}1\}$, $\{10\bar{1}3\}$, and $\{11\bar{2}1\}$ twins also require further examination due to such an ambiguity. In terms of the symmetry of hcp alone, two twinning paths leading to the same twin plane and misorientation are both theoretically reasonable. However, deformation twinning is a symmetry-breaking process [15,16], in which a number of symmetry operations in the parent hcp state are lost (then restored in another way in the product hcp state). It has not been well recognized that the structure of a deformation twin is related to the broken symmetry associated with the deformation process, which is parallel to the nature of topological defects dictated by broken symmetry in other physical systems [16–18].

In this Rapid Communication, we employ a pathway graph approach to investigate the broken symmetry associated with the deformation twinning process in Ti and Zr systems. Symmetry and pathway analyses provide additional information to reduce the number of possible twinning modes, and our theoretical predictions agree with experimental observations. In particular, we demonstrate that the conjugate twinning modes of $\{11\bar{2}2\}/\{11\bar{2}6\}$ are dictated by the broken symmetry, which is another extension twinning mode. Another twinning mode on $\{11\bar{2}1\}$ has been predicted, which is a contraction twin rather than an extension twin. The determination of the twinning path from broken symmetry provides insight to understand the deformation mechanism in Ti and Zr metals/alloys, which also challenges the classical twinning modes suggested in the literature. The graph approach adopted in this Rapid Communication generally applies to all crystal systems, which could be utilized to systematically predict the twinning mechanisms in other metals and alloys.

II. SYMMETRY AND PATHWAY ANALYSES OF hcp TITANIUM AND ZIRCONIUM

Ti and Zr are typical metals that undergo a structural phase transformation between the bcc and hcp phases, which implies a prototype correlation between the broken symmetry and phase transformation path (i.e., the Burgers path between bcc and hcp) [19]. The space group of bcc is $Im\bar{3}m$, which corresponds to a point group of $m\bar{3}m$ with 48 symmetry operations. The space group of hcp is $P6_3mmc$. However, the site symmetry for the occupied Wyckoff position is $\bar{6}m2$, a group with 12 symmetry operations. The preserved symmetry during the bcc → hcp transformation is the intersection group of $m\bar{3}m$ and $\bar{6}m2$ through the Burgers path, which is $mm2$ with four symmetry operations. As a result, there are $48/4 = 12$ equivalent pathways for the bcc → hcp transformation, while there are $12/4 = 3$ equivalent pathways for the hcp → bcc transformation (the atomic structure is shown in Fig. 2), caused by the symmetry breaking [20–22]. The 12 equivalent pathways from bcc → hcp can be easily understood from the symmetry of bcc. Because there are six equivalent $\{110\}_B$ planes in bcc, the bcc lattice can be distorted uniformly into a hexagonal lattice in six equivalent ways, i.e., each $\{110\}_B$ becomes $(0001)_H$, combined with two possible additional shuffles along $\langle 110\rangle_B$ to construct an hcp structure. For simplicity, two hcp states resulting from opposite shuffles will not be distinguished, since they produce the same crystal orientation and the same amount of strain.

Both bcc and hcp are important high-symmetry structural states in the deformation space (i.e., strain space), which dictate the broken symmetries associated with multiple deformation paths. The symmetry groups of bcc and hcp do not have a group-subgroup relation, and they cannot be included in a common finite group. In other words, a crystalline state including both fourfold rotational symmetry and sixfold rotational symmetry is theoretically impossible. Here, we adopt the phase transition graph (PTG) approach to describe interconnected deformation pathways in crystals [23,24]. In a

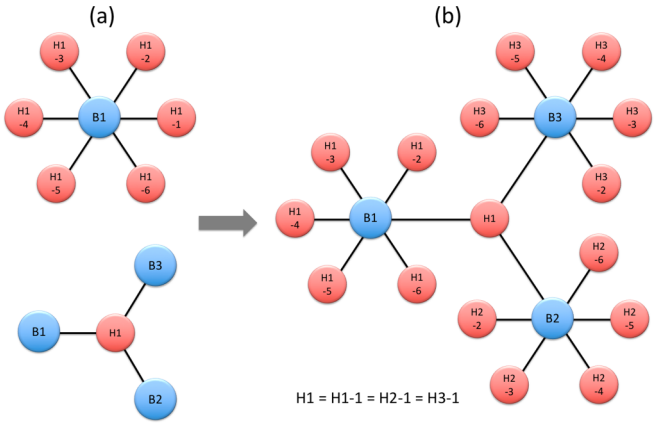

FIG. 3. Phase transition graph for the bcc-hcp transformation: (a) Local structures: Each B vertex is connected with six H vertices, while each H vertex is connected with three B vertices; (b) the global structure generated by combining the local structures.

PTG, each vertex (node) corresponds to a structural state in the deformation space, while each edge (line) between two vertices corresponds to a deformation pathway connecting two structural states.

The PTG for the bcc-hcp transformation system is shown in Fig. 3, in which bcc and hcp structural states are described by blue and red vertices, respectively. As suggested by the above analyses of the broken symmetries during the bcc → hcp and the hcp → bcc transformations, each B vertex is connected with six H vertices (12 is reduced to 6 by ignoring opposite shuffle), while each H vertex is connected with three B vertices [Fig. 3(a)]. The bcc and hcp states are denoted by B and H, while numbers are used to distinguish different structural states in the same phase (e.g., H1-1 and H1-2 describe different hcp states). As a result, when several transformation cycles occur, an interconnected pathway network is expected [Fig. 3(b)]. In particular, the local connectivity between H1 and B1/B2/B3 directly corresponds to the lattice distortion shown in Fig. 2. Because of the non-group-subgroup relation between bcc and hcp, this pathway network is infinite. In practice, we only plot part of the infinite graph. Here, we adopt a double-index system to denote H vertices in Fig. 2(b) based on their directly connected B vertices. For example, we denote the direct H neighbors of B1 as H1-1 through H1-6. Similarly, the six H vertices directly connected to B2 are denoted as H2-1 through H2-6. Since H1 is the common neighbor of B1, B2, and B3, H1 can be denoted equivalently as H1-1, H2-1, and H3-1.

III. DEFORMATION TWINNING IN hcp TITANIUM AND ZIRCONIUM

The PTG shown in Fig. 3 provides an intuitive illustration of the free-energy landscape in the high-dimensional deformation space. Because bcc and hcp are high-symmetry structures, each vertex corresponds to an energy extreme, e.g., maximum, minimum, or saddle point [25], while the vertices in the same type (e.g., hcp) suggest the same energy level. Note that the relative stabilities of different phases depend on temperature in Ti and Zr. At high temperatures (i.e., bcc is stable), bcc vertices correspond to energy minima, while hcp vertices correspond to maxima or saddle points. At low temperatures (i.e., hcp is stable), hcp vertices correspond to minima, while bcc vertices correspond to maxima or saddle points. In the temperature range for phase transformation, all bcc and hcp vertices correspond to minima, with one type as stable and the other as metastable. In particular, when all hcp vertices correspond to minima and all bcc vertices correspond to saddle points (i.e., at the vicinity of the critical temperature T^-) [26], the minimum energy path between two hcp states exactly passes through a bcc saddle. As a result, the deformation path in hcp is directly related to hcp → bcc → hcp. When the temperature further decreases, i.e., lower than the critical temperature ($<T^-$), the bcc saddle gradually becomes a maximum (i.e., a hill on the energy surface), so the minimum energy path would be through a low-symmetry saddle structure (lower symmetry than bcc, e.g., orthorhombic) bypassing the hill. However, since the orthorhombic is a subgroup of bcc, the broken symmetry included in the orthorhombic saddle structure is also included in bcc. Our analyses of the broken symmetry in bcc still lead to the same twinning modes when the symmetry group of the saddle structure is a subgroup of bcc. Such a method has been utilized to investigate the twinning modes in bcc titanium in the literature, which shows that both $\{112\}_B$ and $\{332\}_B$ deformation twin modes are directly related to the broken symmetry associated with the bcc → hcp → bcc path [27,28]. In the Supplemental Material, we also illustrate the method by using a two-dimensional square → hexagon transformation [29], which is fundamentally similar to the bcc → hcp transformation in terms of broken symmetry. In general, the deformation paths in hcp Ti and Zr should be related to not only the symmetry of hcp but also the symmetry of bcc, which provides an additional constraint to greatly reduce the number of possible paths.

By incorporating the above PTG analyses into the twin plane condition [1,7,30], we can systematically predict the possible twinning modes in Ti and Zr. For example, we pick two hcp vertices (e.g., Hi and Hj) and determine their corresponding deformation gradient matrices (e.g., $\mathbf{F}_{\mathrm{H}i}$ and $\mathbf{F}_{\mathrm{H}j}$),

$$\mathbf{Q}\mathbf{F}_{\mathrm{H}j} - \mathbf{F}_{\mathrm{H}i} = s(\eta \otimes \mathbf{K}). \tag{1}$$

$\boldsymbol{\eta}$ is the twinning shear direction, and $\mathbf{K}$ is twin plane normal. s is the shear magnitude. $\mathbf{Q}$ is a rigid-body rotation matrix, which captures the misorientation between two twin-related domains. Equation (1) usually has two conjugate solutions, as described by $\mathbf{K}_1/\boldsymbol{\eta}_1$ and $\mathbf{K}_2/\boldsymbol{\eta}_2$. Depending on the rational/irrational nature of the twin plane index, the two solutions could be both compound twins, or type I and type II twins, as classified in the literature [1,7]. In this Rapid Communication, all the twin boundary solutions are obtained by solving Eq. (1), with different choices of $\mathbf{F}_{\mathrm{H}i}$ and $\mathbf{F}_{\mathrm{H}j}$. The mathematical procedures to solve Eq. (1) can be found in the literature [7,31]. The deformation gradient matrices for all structural states (i.e., all vertices in Fig. 3) are listed in the Supplemental Material [29].

For convenience, the major twinning modes obtained from previous theoretical calculations in the literature are listed in

TABLE I. Twinning modes theoretically predicted in the literature (for hcp titanium).

Type No.	$\mathbf{K}_1/\boldsymbol{\eta}_1$ misorientation	$\mathbf{K}_2/\boldsymbol{\eta}_2$ misorientation	Shear s	Extension/ Contraction
1	$(\bar{1}102)/[1\bar{1}01]$ 85.0° about $[11\bar{2}0]$	$(\bar{1}10\bar{2})/[1\bar{1}0\bar{1}]$ 85.0° about $[11\bar{2}0]$	0.175	E
2	$(\bar{1}01\bar{1})/[\bar{1}012]$ 57.2° about $[2\bar{1}\bar{1}0]$	$(10\bar{1}\bar{3})/[30\bar{3}2]$ 62.8° about $[2\bar{1}\bar{1}0]$	0.098	C
3	$(11\bar{2}2)/[11\bar{2}\bar{3}]$ 64.4° about $[1\bar{1}00]$	$(\bar{1}\bar{1}24)/[\bar{2}\bar{2}4\bar{3}]$ 76.9° about $[1\bar{1}00]$	0.218	C
4	$(11\bar{2}1)/[\bar{1}\bar{1}26]$ 35.0° about $[1\bar{1}00]$	$(0001)/[\bar{1}\bar{1}20]$ 0°	0.630	E

Table I (for hcp Ti) [1,8]. There are four major types of conjugate twinning pairs. The first one is $\{10\bar{1}2\}/\langle 10\bar{1}\bar{1}\rangle$, which is the most frequently observed to be a twin in hcp crystals. The second one is the conjugate pair of $\{10\bar{1}1\}/\langle 10\bar{1}\bar{2}\rangle$ and $\{10\bar{1}\bar{3}\}/\langle 30\bar{3}2\rangle$, which is usually considered as the origin of the observed $\{10\bar{1}1\}$ and $\{10\bar{1}\bar{3}\}$ twins. The third one explains the observed $\{11\bar{2}2\}$ twin, but there is still a controversial issue about its conjugate $\{11\bar{2}\bar{4}\}$. The fourth one is usually considered as the origin of the observed $\{11\bar{2}1\}$ twin. The above results are summarized in Christian and Mahajan's classical review paper [1].

We choose two hcp structural states in Fig. 3, and use their deformation gradient matrices in Eq. (1). In particular, we focus on the twin formation between two hcp vertices with a path through one bcc vertex (e.g., the path between H1-1 and H2 through B1), and those with a path through two bcc vertices (e.g., the path between H1-2 and H2-2 through B1/H1/B2). All predicted twinning modes in hcp Ti ($c/a = 1.587$) and Zr ($c/a = 1.593$) are listed in Tables II and III, respectively. Most of our results are distinctively different from the previous ones in terms of twinning shear vectors, but they coincide in twin plane and misorientation. The general crystallographic phenomena, different twinning paths leading to identical twin boundaries and misorientations, exist in typical $\{11\bar{2}2\}$, $\{10\bar{1}1\}$, $\{10\bar{1}3\}$, and $\{11\bar{2}1\}$ twins in hcp crystals.

Note that the $\{10\bar{1}2\}/\langle 10\bar{1}\bar{1}\rangle$ twinning mode is the only mode that can be found in both Tables I and II. All other predictions in Table II are significantly different from those in Table I. For example, for the $\{11\bar{2}2\}$ twin with a 64.4° misorientation, our prediction suggests a $(\bar{1}\bar{1}2\bar{6})/[11\bar{2}\bar{1}]$ conjugate mode, which is different from $(\bar{1}\bar{1}24)/[\bar{2}\bar{2}4\bar{3}]$ in the literature [1]. In fact, a recent experimental observation of a $(\bar{1}\bar{1}2\bar{6})$ twin does support our prediction, which is also phenomenologically equivalent to a double twinning mechanism proposed in the literature [9,10]. For the $\{10\bar{1}1\}$ twin with a 57.2° misorientation, our prediction suggests an irrational $[\overline{0.38}\ 1\ \overline{0.62}\ 0.25]$ twin shear, which is different from $[\bar{1}012]$ suggested in the literature [1]. For the $\{10\bar{1}3\}$ twin with a 62.8° misorientation, our prediction suggests a $[\overline{0.37}\ 1\ \overline{0.63}\ 0.09]$ twin shear, which is different from $[30\bar{3}2]$ suggested in the literature [1]. For the $\{11\bar{2}1\}$ twin with a 35.0° misorientation, our prediction suggests a $[0.83\ 0.17\ \bar{1}\ 0.51]$ twin shear, which is different from $[\bar{1}\bar{1}26]$ suggested in the literature [1]. Please recall the twinning path ambiguity as shown in Fig. 1. In the literature, experimental observations of twin planes and misorientations in hcp [32,33] cannot uniquely determine a deformation path, so they do not provide enough information to

TABLE II. Twinning mode predictions in hcp titanium (E/C stands for extension/contraction twin).

State i	State j	$\mathbf{K}_1/\boldsymbol{\eta}_1$ misorientation	$\mathbf{K}_2/\boldsymbol{\eta}_2$ misorientation	Shear s	E/C	Other states i,j
H1	H2	$(\bar{1}102)/[1\bar{1}01]$ 85.0° about $[11\bar{2}0]$	$(\bar{1}10\bar{2})/[1\bar{1}0\bar{1}]$ 85.0° about $[11\bar{2}0]$	0.175	E	H3/H4 H5/H6
H1	H3	$(10\bar{1}\bar{1})/[\overline{0.38}\ 1\ \overline{0.62}\ 0.25]$ 57.2° about $[\bar{1}2\bar{1}0]$	$(0.24\ \bar{1}\ 0.76\ \overline{0.28})/[\bar{5}143]$ 65.3° about $[\bar{1}\ 2\ \bar{1}\ \overline{0.60}]$	0.343	C	H1/H4 H1/H5 H1/H6
H1-2	H2-2	$(\bar{1}\bar{1}22)/[11\bar{2}3]$ 64.4° about $[\bar{1}100]$	$(\bar{1}\bar{1}2\bar{6})/[11\bar{2}\bar{1}]$ 55.8° about $[\bar{1}100]$	0.152	E	
H1-3	H2-4	$(\bar{1}2\bar{1}\bar{1})/[0.83\ 0.17\ \bar{1}\ 0.51]$ 35.0° about $[\bar{1}010]$	$(\overline{0.97}\ \overline{0.66}\ 1.62\ \bar{1})/[5\bar{7}23]$ 54.6° about $[\bar{1}\ 0\ 1\ 0.60]$	0.515	C	H1-5/H2-6
H1-3	H2-6	$(\bar{1}\bar{2}3\bar{5})/[0.26\ \bar{1}\ 0.74\ 0.80]$ 88.2° about $[\bar{4}5\bar{1}0]$	$(\overline{0.16}\ 1\ \overline{0.84}\ \overline{0.84})/[11\bar{2}3]$ 64.4° about $[\bar{1}100]$	0.485	C	H1-5/H2-4
H1-4	H2-3	$(10\bar{1}\bar{3})/[\overline{0.37}\ 1\ \overline{0.63}\ 0.09]$ 62.8° about $[1\bar{2}10]$	$(0.24\ \bar{1}\ 0.76\ 0.24)/[\bar{2}113]$ 64.4° about $[0\bar{1}10]$	0.562	E	H1-6/H2-5
H1-4	H2-5	$(10\bar{1}\bar{1})/[\bar{1}2\bar{1}0]$ 0°	$(1\bar{4}31)/[\bar{1}\ 0.36\ 0.64\ 0.49]$ 32.6° about $[2\bar{1}\bar{1}3]$	0.658	E	

TABLE III. Twinning mode predictions in hcp zirconium (E/C stands for extension/contraction twin).

State i	State j	$\mathbf{K}_1/\boldsymbol{\eta}_1$ misorientation	$\mathbf{K}_2/\boldsymbol{\eta}_2$ misorientation	Shear s	E/C	Other states i,j
H1	H2	$(\bar{1}102)/[1\bar{1}01]$ 85.2° about $[11\bar{2}0]$	$(\bar{1}10\bar{2})/[1\bar{1}0\bar{1}]$ 85.0° about $[11\bar{2}0]$	0.168	E	H3/H4 H5/H6
H1	H3	$(10\bar{1}\bar{1})/[\overline{0.37}\ 1\ \overline{0.63}\ 0.26]$ 57.1° about $[\bar{1}2\bar{1}0]$	$(0.23\ \bar{1}\ 0.77\ \overline{0.31})/[\bar{5}143]$ 65.5° about $[\bar{1}\ 2\ \bar{1}\ \overline{0.59}]$	0.345	C	H1/H4 H1/H5 H1/H6
H1-2	H2-2	$(\bar{1}\bar{1}22)/[11\bar{2}3]$ 64.2° about $[\bar{1}100]$	$(\bar{1}\bar{1}2\bar{6})/[11\bar{2}\bar{1}]$ 55.9° about $[\bar{1}100]$	0.145	E	
H1-3	H2-4	$(\bar{1}2\bar{1}\bar{1})/[0.83\ 0.17\ \bar{1}\ 0.52]$ 34.9° about $[\bar{1}010]$	$(\overline{0.94}\ \overline{0.65}\ 1.59\ \bar{1})/[5\bar{7}23]$ 54.8° about $[\bar{1}\ 0\ 1\ 0.59]$	0.517	C	H1-5/H2-6
H1-3	H2-6	$(\bar{1}\bar{2}3\bar{5})/[0.25\ \bar{1}\ 0.75\ 0.80]$ 88.5° about $[\bar{4}5\bar{1}0]$	$(\overline{0.15}\ 1\ \overline{0.85}\ \overline{0.85})/[11\bar{2}3]$ 64.2° about $[\bar{1}100]$	0.492	C	H1-5/H2-4
H1-4	H2-3	$(10\bar{1}\bar{3})/[\overline{0.36}\ 1\ \overline{0.64}\ 0.09]$ 63.0° about $[1\bar{2}10]$	$(0.23\ \bar{1}\ 0.77\ 0.23)/[\bar{2}113]$ 64.2° about $[0\bar{1}10]$	0.562	E	H1-6/H2-5
H1-4	H2-5	$(10\bar{1}\bar{1})/[\bar{1}2\bar{1}0]$ 0°	$(1\bar{4}31)/[\bar{1}\ 0.36\ 0.64\ 0.49]$ 32.6° about $[2\bar{1}\bar{1}3]$	0.657	E	

distinguish our predictions and those in the literature [1]. However, since the twinning strains associated with different deformation paths are different, they could make distinctive effects on the c axis (i.e., extension or contraction twin). In our predictions, $\{10\bar{1}3\}$ and $\{11\bar{2}2\}$ are extension twins, and $\{11\bar{2}1\}$ is a contraction twin, which are clearly different from those suggested in the literature [5]. As a consequence, it is important to identify the extension twin and contraction twin from different loading conditions in the experiments, which could provide critical information to determine the twinning path.

Because the twinning modes predicted in this study originate from the broken symmetry from bcc to hcp, they could generally exist in metals with a bcc → hcp transformation, i.e., a number of metals/alloys in groups 3 and 4 in the periodic table (such as Sc, Y, Gd, Ti, Zr, Hf, etc.). From a crystal symmetry point of view, those metals/alloys with the bcc → hcp transformation are not distinguished (except different lattice parameters). In addition, our pathway method can be generally applied to other materials with structural phase transformations (e.g., Fe alloys with a fcc/bcc transformation, Ti alloys with a bcc/hcp transformation, Co alloys with a fcc/hcp transformation). As demonstrated in the literature, the deformation twin modes in fcc Fe, bcc Fe, and bcc Ti have been predicted through the pathway approach [17,28,34,35], and the results agree with experimental observations.

IV. CONCLUSIONS

By using a pathway graph approach, we demonstrate that the deformation twinning in hcp Ti and Zr is dictated by not only the symmetry of hcp, but also the broken symmetry from bcc to hcp. Our theoretical predictions not only agree with experimental observations, but also challenge the classical twinning modes suggested in the literature. Based on our calculations, we suggest to identify the extension twin and contraction twin from different loading conditions in the experiments, which could provide critical information to determine the twinning path. Our method to determine the deformation twinning path from broken symmetry will provide insight to understand the deformation mechanism in Ti and Zr metals/alloys.

ACKNOWLEDGMENTS

We sincerely thank Dr. Cyril Cayron (EPFL) for sharing his knowledge on hcp twinning and having fruitful discussions with us. This work was supported by the U.S. Department of Energy, at Idaho National Laboratory operated by Battelle Energy Alliance (BEA) under DOE-NE Idaho Operations Office Contract No. DE-AC07-05ID14517. Y.Z. would also like to acknowledge the financial support by the startup funding from the Department of Chemical and Materials Engineering at University of Nevada, Reno.

[1] J. W. Christian and S. Mahajan, Deformation twinning, Prog. Mater. Sci. **39**, 1 (1995).

[2] J. W. Christian, *The Theory of Transformations in Metals and Alloys*, 3rd ed. (Elsevier, Oxford, UK, 2002).

[3] Q. Yu, Z. W. Shan, J. Li, X. Huang, L. Xiao, J. Sun, and E. Ma, Strong crystal size effect on deformation twinning, Nature (London) **463**, 335 (2010).

[4] Y. T. Zhu, X. Z. Liao, and X. L. Wu, Deformation twinning in nanocrystalline materials, Prog. Mater. Sci. **57**, 1 (2012).

[5] M. H. Yoo and J. K. Lee, Deformation twinning in hcp metals and alloys, Philos. Mag. A **63**, 987 (1991).

[6] J. Wang, Q. Yu, Y. Jiang, and I. J. Beyerlein, Twinning-associated boundaries in hexagonal close-packed metals, JOM **66**, 95 (2014).

[7] C. Cayron, Complements to Mügge and Friedel's theory of twinning, Metals **10**, 231 (2020).

[8] A. G. Crocker and M. Bevis, The crystallography of deformation twinning in titanium, in *The Science, Technology*

and Application of Titanium (Pergamon, Oxford, U.K., 1970), pp. 453–458.

[9] A. Ostapovets, J. Buršík, K. Krahula, L. Král, and A. Serra, On the relationship between and conjugate twins and double extension twins in rolled pure Mg, Philos. Mag. **97**, 1088 (2017).

[10] C. Cayron, A one-step mechanism for new twinning modes in magnesium and titanium alloys modelled by the obliquity correction of a $(58^{\circ}, a+2b)$ prototype stretch twin, Acta Crystallogr., Sect. A **74**, 44 (2018).

[11] J. Wang, I. J. Beyerlein, J. P. Hirth, and C. N. Tomé, Twinning dislocations on $\{\bar{1}011\}$ and $\{\bar{1}013\}$ planes in hexagonal close-packed crystals, Acta Mater. **59**, 3990 (2011).

[12] C. Cayron and R. Logé, Evidence of new twinning modes in magnesium questioning the shear paradigm, J. Appl. Crystallogr. **51**, 809 (2018).

[13] B. Li, Reply to the two Comments, by A. Serra, D. J. Bacon, and R. C. Pond, and by H. El Kadiri and C. Barrett on B. Li, H. El Kadiri, and M. F. Horstemeyer, Extended zonal dislocations mediating $\{11\bar{2}2\}\langle 11\bar{2}\bar{3}\rangle$ twinning in titanium, Philos. Mag. **93**, 3504 (2013).

[14] J. Wang, S. K. Yadav, J. P. Hirth, C. N. Tomé, and I. J. Beyerlein, Pure-shuffle nucleation of deformation twins in hexagonal-close-packed metals, Mater. Res. Lett. **1**, 126 (2013).

[15] Y. Gao, Symmetry and pathway analyses of the twinning modes in Ni-Ti shape memory alloys, Materialia **6**, 100320 (2019).

[16] N. D. Mermin, The topological theory of defects in ordered media, Rev. Mod. Phys. **51**, 591 (1979).

[17] Y. Gao, Y. Wang, and Y. Zhang, Deformation pathway and defect generation in crystals: a combined group theory and graph theory description, IUCrJ **6**, 96 (2019).

[18] Y. Gao, A Cayley graph description of the symmetry breaking associated with deformation and structural phase transitions in metallic materials, Materialia **9**, 100588 (2020).

[19] W. G. Burgers, On the process of transition of the cubic-body-centered modification into the hexagonal-close-packed modification of zirconium, Physica **1**, 561 (1934).

[20] C. Cayron, The transformation matrices (distortion, orientation, correspondence), their continuous forms and their variants, Acta Crystallogr., Sect. A **75**, 411 (2019).

[21] Y. Gao, R. Shi, J. F. Nie, S. A. Dregia, and Y. Wang, Group theory description of transformation pathway degeneracy in structural phase transformations, Acta Mater. **109**, 353 (2016).

[22] C. Cayron, Continuous atomic displacements and lattice distortion during fcc-bcc martensitic transformation, Acta Mater. **96**, 189 (2015).

[23] Y. Gao, S. A. Dregia, and Y. Wang, A universal symmetry criterion for the design of high performance ferroic materials, Acta Mater. **127**, 438 (2017).

[24] Y. Gao, Y. Zhang, B. W. Beeler, and Y. Wang, Self-organized multigrain patterning with special grain boundaries produced by phase transformation cycling, Phys. Rev. Mater. **2**, 073402 (2018).

[25] A.G. Khachaturyan, *Theory of Structural Transformations in Solids* (Wiley-Interscience, New York, 1983).

[26] F. Falk, Landau theory and martensitic phase transitions, J. Phys. Colloq. **43**, C4-3 (1982).

[27] P. Castany, Y. Yang, E. Bertrand, and T. Gloriant, Reversion of a Parent $\{130\}\langle 310\rangle_{\alpha''}$ Martensitic Twinning System at the Origin of $\{332\}\langle 113\rangle_{\beta}$ Twins Observed in Metastable β Titanium Alloys, Phys. Rev. Lett. **117**, 245501 (2016).

[28] S. Antonov, Z. Kloenne, Y. Gao, D. Wang, Q. Feng, Y. Wang, H. L. Fraser, and Y. Zheng, Novel deformation twinning system in a cold rolled high-strength metastable-β Ti-5Al-5V-5Mo-3Cr-0.5 Fe alloy, Materialia **9**, 100614 (2020).

[29] See Supplemental Material at http://link.aps.org/supplemental/10.1103/PhysRevMaterials.4.070601 for deformation pathway and deformation gradient matrix calculations.

[30] C. M. Wayman, *Introduction to the Crystallography of Martensitic Transformation, Macmillan Series in Materials Science* (Macmillan, New York, 1964).

[31] K. Bhattacharya, *Microstructure of Martensite: Why it Forms and How it Gives Rise to the Shape-Memory Effect* (Oxford University Press, Oxford, UK, 2003), Vol. 2.

[32] J. C. Williams, R. G. Baggerly, and N. E. Paton, Deformation behavior of HCP Ti-Al alloy single crystals, Metall. Mater. Trans. A **33**, 837 (2002).

[33] X. Li, Y. L. Duan, G. F. Xu, X. Y. Peng, C. Dai, L. G. Zhang, and Z. Li, EBSD characterization of twinning in cold-rolled CP-Ti, Mater. Charact. **84**, 41 (2013).

[34] Y. Gao and Y. Wang, Hidden pathway during fcc to bcc/bct transformations: Crystallographic origin of slip martensite in steels, Phys. Rev. Mater. **2**, 093611 (2018).

[35] Y. Gao, Y. Zhang, and Y. Wang, Determination of twinning path from broken symmetry: A revisit to deformation twinning in bcc metals, Acta Mater. (2020), doi:10.1016/j.actamat.2020.06.031.